

# Numerical investigation of truck aerodynamics on several classes of infrastructures

A. Alonso-Estébanez<sup>a,\*</sup>, J.J. del Coz Díaz<sup>b</sup>, F.P. Álvarez Rabanal<sup>b</sup>, P. Pascual-Muñoz<sup>a</sup> and P.J. García Nieto<sup>c</sup>.

<sup>a</sup> Department of Transport, Projects and Process Technology, University of Cantabria, Avda. Los Castros s/n, 39005 Santander, Spain.

<sup>b</sup> Department of Construction, GICONSIME Research Team, University of Oviedo, Departmental Building 7, 33204 Gijón, Spain.

<sup>c</sup> Department of Mathematics, Faculty of Sciences, University of Oviedo, 33007 Oviedo, Spain.

## Abstract

This paper describes the effect of different testing parameters (configuration of infrastructure and truck position on road) on truck aerodynamic coefficients under cross wind conditions, by means of a numerical approach known as Large Eddy Simulation (LES). In order to estimate the air flow behaviour around both the infrastructure and the truck, the filtered continuity and momentum equations along with the Smagorinsky–Lilly model were solved. A solution for these non-linear equations was approached through the finite volume method (FVM) and using temporal and spatial discretization schemes. As for the results, the aerodynamic coefficients acting on the truck model exhibited nearly constant values regardless of the Reynolds number. The flat ground is the infrastructure where the rollover coefficient acting on the truck model showed lowest values under cross wind conditions (yaw angle of 90°), while the worst infrastructure studied for vehicle stability was an embankment with downward-slope on the leeward side. The position of the truck on the road and the value of embankment slope angle that minimizes the rollover coefficient were determined by successfully applying the Response Surface Methodology.

*Keywords:* Cross wind; Embankments; Heavy vehicles aerodynamics; Large Eddy Simulation (LES); Finite Volume Method (FVM); Computational Fluid Dynamics (CFD).

## 1. Introduction

As a consequence of cross wind induced accidents in road/rail transportation, the amount of research on this issue has increased over the last years (Baker and Reynolds, 1992; Bettel et al., 2003; Bocciolone et al., 2008). Several accidents due to cross wind have been registered and analysed worldwide (Coleman and Baker, 1990; Imai et al., 2002; Shao et al., 2011). High-sided vehicles such as trucks, caravans and trains are especially affected by cross wind since the risk of rollover is higher than for other kinds of vehicles (Dorigatti et al., 2012). In addition, new vehicles are designed to be lighter to reduce their energy consumption and this aspect negatively affects their stability during driving (Alvarez-Legazpi et al., 2010).

The overturning risk associated with cross wind mainly depends on local wind characteristics and the dynamic behavior of vehicles. The local wind characteristics are influenced by the infrastructure scenario along transportation routes (Suzuki et al., 2003; Cheli et al., 2010). At locations such as embankments, bridges and tunnel exits, vehicles have more susceptibility to rollover than in other places. Therefore, better knowledge of the stability of

---

\* Corresponding author, Ph.D., E-mail address: alonsoea@unican.es.

43 vehicles by measuring the aerodynamic coefficients in these scenarios may improve the safety  
44 regulations in cross wind conditions. For this reason, several methodologies have been used by  
45 different researchers to analyze the stability of high-sided vehicles under cross wind conditions  
46 in these risky infrastructures.

47 Dorigatti et al. (2012) carried out wind tunnel tests to obtain the aerodynamic loads of three  
48 kinds of vehicles located on two models of bridge. Other research has been focused on vehicle  
49 stability in special bridge locations such as bridge towers (Argentini et al., 2011; Ma et al.,  
50 2016; Wu et al., 2017). This is because the towers cause sudden changes in the aerodynamic  
51 loads of the vehicles. Moreover, the effect of embankments on the overturning risk of vehicles  
52 has been analyzed in several studies (Diedrichs et al., 2007; Miao et al., 2010; Schober et al.,  
53 2010) due to the wind speed increasing on upslopes (Bitsuamlak et al., 2004).

54 This knowledge of unstable aerodynamic loads acting on vehicles for different scenarios has  
55 been used for the development of wind warning systems to protect high-speed trains against  
56 strong cross winds (Hoppmann et al., 2002; Delaunay et al., 2006). Other studies focus on the  
57 optimization of barriers to improve the protection of vehicles against cross wind conditions  
58 (Yang et al., 2017). So far, different techniques such as numerical simulation, wind tunnel  
59 testing and full scale experiments have been used to evaluate vehicle stability under cross wind  
60 conditions. For instance, Hibino et al. (2010) carried out a full-scale experiment to validate the  
61 equation that is applied to solve the overturning problem of a rigid body. Wind tunnel tests were  
62 performed by Bocciolone et al. (2008) to analyze the most critical conditions in several road  
63 infrastructures as a result of cross wind action. Sterling et al. (2010) contrasted the results of  
64 aerodynamic loads acting on a truck by using the three techniques cited above.

65 In this paper, the aerodynamic coefficients of a truck model in different scenarios and  
66 subjected to cross wind conditions are obtained by means of numerical simulation. This study  
67 aims to analyze how different configurations of embankments affect vehicle stability by using a  
68 validated numerical model in combination with a design of experiments (DOE) methodology.  
69 This methodology enables scenarios to be distinguished in which risk of rollover accident due to  
70 cross wind action is especially relevant. This information can be very useful for making relevant  
71 decisions in terms of traffic safety improvement (use of wind fences, new regulations, etc.).  
72 Moreover, a better understanding of how different geometric parameters of embankments affect  
73 the aerodynamics of the vehicle can be very valuable for the design of road structures with  
74 reduced risk of rollover accidents. The first section of the paper describes the CFD model and  
75 its numerical setup while the second analyzes the results provided by the numerical simulation.  
76 Finally, the most important conclusions are drawn based on the results obtained.

77

## 78 2. Numerical procedure

### 79 2.1. Mathematical approach

80 Cross winds that negatively influence vehicle stability are characterized by a turbulent  
81 regime, which consists of eddies with a wide range of length and time scales. It is possible to  
82 solve the whole spectrum of turbulent scales by applying the method known as direct numerical  
83 simulation (DNS). However, the high computational cost required to solve common engineering  
84 problems by using the DNS approach makes this unfeasible (ANSYS FLUENT, 2017). With  
85 another approach known as Large Eddy Simulation (LES) only large eddies are solved directly  
86 whereas the small eddies are solved using turbulence models. Therefore, LES enables the use of  
87 coarser grids and larger time steps in comparison to DNS, as well as finer grids than those used  
88 in models solved with the Reynolds-Averaged Navier–Stokes equations approach (RANS). All  
89 turbulent scales are modeled in RANS; therefore, LES allows more accurate results to be  
90 obtained than RANS, particularly for cases where significant unsteadiness in the large scale of  
91 flow are generated, as could happen around trucks under cross wind conditions. Accordingly,  
92 the LES approach was used to carry out the 3D numerical simulation presented in this work.

93 The LES approach was also used in other studies to analyze the effect of cross wind conditions  
 94 on the stability of vehicles such as cars and trains (Tsubokura et al., 2010; García et al., 2015;  
 95 Dragomirescu et al., 2016).

96 The LES approach filters the Navier-Stokes equations and resolves these equations for the  
 97 large-scale eddies. The filtered continuity and momentum equations for an incompressible flow  
 98 are:

$$\frac{\partial}{\partial x_i}(\rho \bar{u}_i) = 0 \quad (1)$$

$$\frac{\partial}{\partial t}(\rho \bar{u}_i) + \frac{\partial}{\partial x_j}(\rho \bar{u}_i \bar{u}_j) = \frac{\partial}{\partial x_j}(\sigma_{ij}) - \frac{\partial \bar{p}}{\partial x_i} - \frac{\partial \tau_{ij}}{\partial x_j} \quad (2)$$

99 where  $\bar{u}_i$  and  $\bar{p}$  are the filtered component of velocity in the  $i$  direction and pressure,  
 100 respectively;  $\sigma_{ij}$  is the stress tensor due to molecular viscosity; and  $\tau_{ij}$  is the subgrid-scale  
 101 turbulent stress tensor. In order to obtain the term  $\tau_{ij}$ , the Boussinesq assumption was  
 102 considered and the Smagorinsky–Lilly model (Smagorinsky, 1963) was employed. Detailed  
 103 information about these equations can be found in ANSYS FLUENT, (2017).  
 104

105 The finite volume method (FVM) is applied to solve the equations described above, which  
 106 detail the transport of the main properties of turbulent flow. The geometric domain is divided  
 107 into a finite number of cells with nodal points. The virtual control volumes are cell-centered and  
 108 are directly delimited by the grid nodes, and the variables' values will only be available at the  
 109 center of cells. The governing equations that describe the conservation of a general variable of  
 110 flow  $\phi$  (e.g. components of the flow velocity  $u$ , or pressure) are integrated within the control  
 111 volumes.

112 In this research work, a bounded second-order implicit scheme was used for time  
 113 discretization. Regarding spatial discretization, the following schemes were used: Least Squares  
 114 Cell-Based to calculate gradients; second order to calculate the pressure gradient term; and  
 115 bounded central differencing to solve the convection-diffusion equations. The SIMPLE  
 116 algorithm of Patankar and Spalding (1972) was used to solve pressure–velocity coupling. This  
 117 is a recommended configuration for single-phase problems using either the pressure-based or  
 118 density-based solver (ANSYS FLUENT, 2017). The time step was set based on the ratio  
 119 between the vehicle width and the upstream wind velocity obtained at the level of the vehicle  
 120 (Wang, 2014). Therefore, the time step was defined as:

$$\Delta t = 0.1 \frac{W}{U} \quad (3)$$

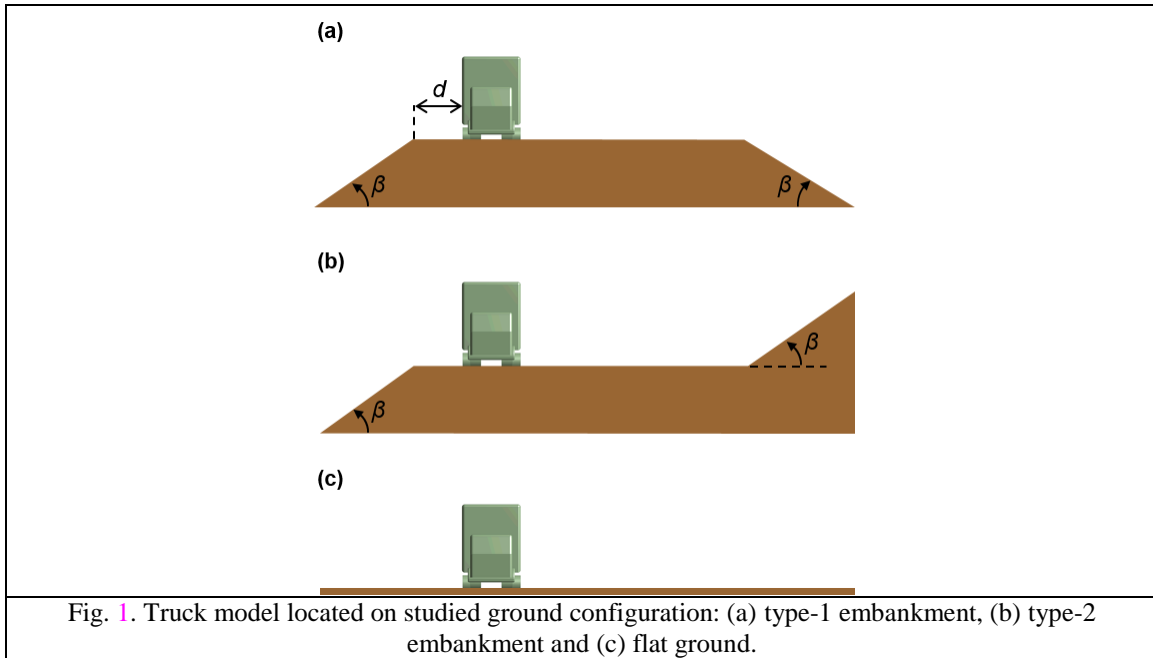
121 where  $W$  is the width of vehicle and  $U$  is the upstream wind velocity. The Courant–  
 122 Friedrichs–Lewy number (CFL) was below one in most of the cells for the time step used. The  
 123 flow covered three times the domain before the results were sampled. The aerodynamic  
 124 coefficients were averaged during  $2300\Delta t$ , which is the time required by the air flow to cover  
 125 three times the domain.

126 Finally, the algebraic equation system was solved by using an iterative method. A converged  
 127 solution was reached when the following requirements were met (ERCOFTAC, 2000): scaled  
 128 residuals of all the variables below  $1 \cdot 10^{-4}$  and constant value (4 significant figures) of the  
 129 monitored aerodynamic coefficient. To carry out the simulations, a server with Intel Xeon 5630  
 130 @ 2.53 GHz (16 processors) CPU, 64 GB RAM memory and 4 TB hard disk was used that  
 131 worked under the Windows server 2003 operating system.  
 132

133

134 **2.2. Infrastructure models**

135 In order to analyze the effect of the infrastructure scenarios on the aerodynamic coefficients  
136 involved in the rollover of a truck, three stationary ground configurations were proposed for  
137 study (see Fig. 1): embankment with downward-slope on the leeward side (type-1  
138 embankment), embankment with upward-slope on the leeward side (type-2 embankment) and  
139 flat ground. Height, slope angles and road width have the same dimensions in both embankment  
140 scenarios (see Fig. 1). Detailed information about these dimensions as well as about those of the  
141 truck can be found in Cheli et al. (2011a, b).



142 To carry out the numerical simulation, the three-dimensional domain representing the  
143 regions of air around the truck has to be built (see Fig. 2). The upstream and downstream  
144 distances from the bluff bodies (truck and embankment models) in the three scenarios are at  
145 least  $6H_{obs}$  ( $H_{obs}$  being the obstacle height) and  $14.4H_{obs}$ , respectively (see Fig. 2). The cross  
146 section has the same dimensions as the boundary layer test section used in the wind tunnel  
147 located in the Polytechnic of Milan: 14 m x 4 m (Bocciolone et al., 2008). In addition, the  
148 domain was divided into three sub-domains (near domain and two far domains) for several  
149 reasons. The near domain surrounding the truck model was defined in order to build a finer grid  
150 in this region, which enables the precise capture of the gradients of the flow variables in the  
151 proximity of the truck and infrastructures. The remaining domain was divided into two sub  
152 domains to set different values in the inlet boundary condition (see Fig. 2).

153 **2.3. Grid and boundary conditions**

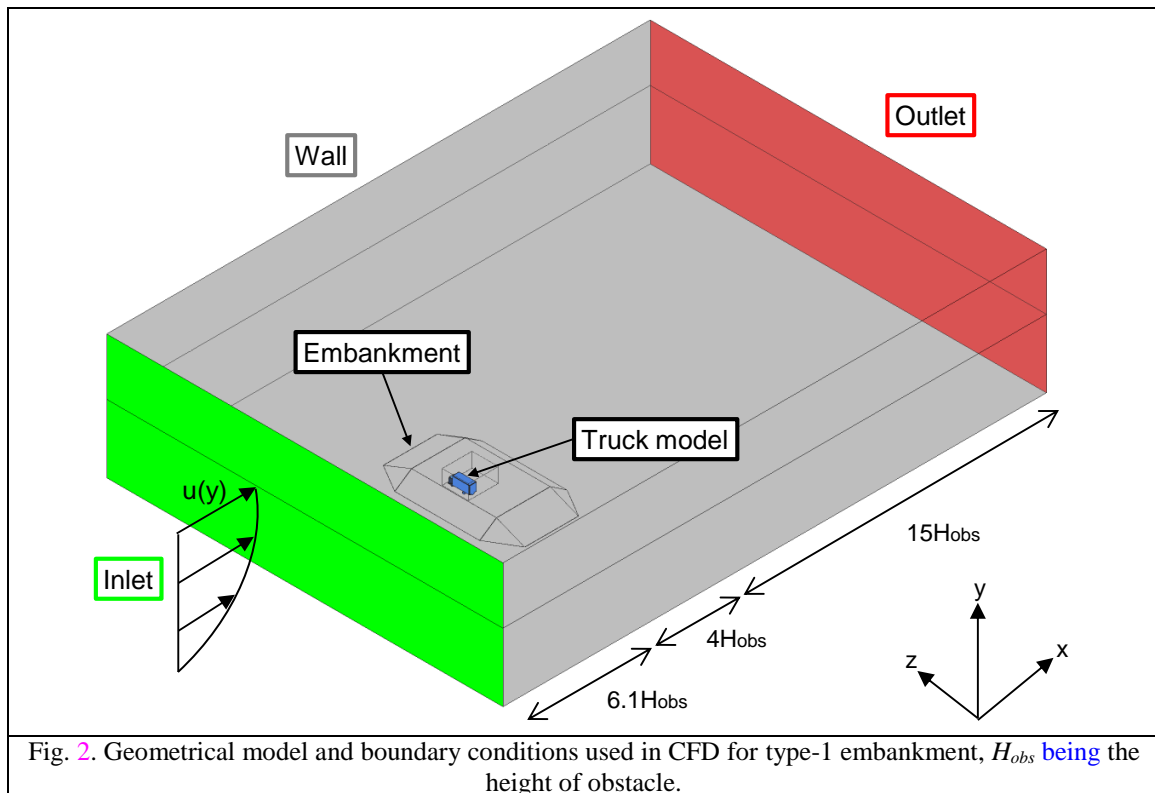
155 Three kinds of grid were used in the CFD models: inflation grid for the regions of fluid close  
156 to solid surfaces (infrastructures, walls of test section and truck), tetrahedral grid for far  
157 domain.1 and near domain and structural grid for far domain.2 (Fig. 3). The inflation grid  
158 enables the high gradients of the variables in the region of the boundary layer to be represented  
159 with a greater accuracy. The inflation grid consists of ten inflated layers with a growth rate of  
160 1.2, the thickness of the first layer being calculated to obtain a  $y^+$  value of 1. The variable  $y^+$  is  
161 the dimensionless distance from the wall and is calculated as follows:  
162

$$y^+ = \frac{u_\tau \cdot y}{\nu} \quad (4)$$

163 Where  $y$  is the distance from the wall;  $u_\tau$  is the shear velocity; and  $\nu$  the kinematic viscosity.

164 The grid size used to solve the CFD models varied from 11.87 million to 20.05 cells for the  
 165 flat ground and type-1 embankment, respectively. **The boundary conditions adopted for solving**  
 166 **the numerical model are the following** (see Fig. 2) (Tu et al., 2012; Madenci and Guven, 2015;  
 167 Yang et al., 2017):

- 168 • **Inlet:**  $U(z)$  was defined according to the wind speed profile **introduced** in Cheli et al.  
 169 (2011a, b) for low turbulence condition, where the free stream velocity,  $U_\infty$ , was equal  
 170 to 13.9 m/s. The components of the wind speed in **the**  $Y$  and  $Z$  directions are zero  
 171 ( $V, W=0$ ). The fluctuating inflow was generated with the Spectral synthesizer (SS)  
 172 method proposed by Kraichnan (1970) and modified by Smirnov et al. (2001). This  
 173 method randomly synthesizes a divergence-free velocity field from the summation of  
 174 Fourier harmonics to generate fluctuations of the velocity components (ANSYS  
 175 FLUENT, 2017). **The turbulent length scale  $l$ , and the turbulence intensity  $I$ , were**  
 176 **adjusted to 0.1m and 2%**, respectively, as in Cheli et al. (2011a, b).
- 177 • **Outlet:** Relative pressure  $p = 0$ . At the outlet boundary  $\Gamma_{out}$ , the normal gradients of all  
 178 variables are set to zero, which corresponds to the Neumann boundary condition.
- 179 • **Solid walls:** A non-slip condition ( $U, V, W=0$ ) was adopted **at** the solid surface of **the**  
 180 domain (walls of test section, surfaces of both infrastructures and truck), **as seen** in Fig.  
 181 **2.**





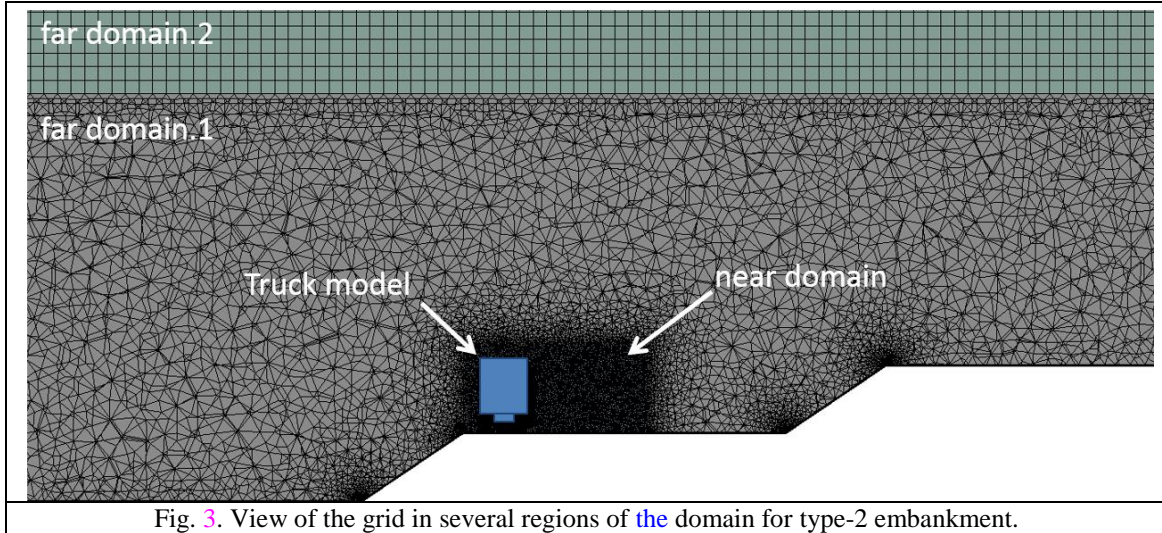


Fig. 3. View of the grid in several regions of the domain for type-2 embankment.

183  
184

#### 2.4. Evaluation of aerodynamic loads and moments

185 The aerodynamic loads and moments acting on the truck are side force ( $F_S$ ), lift force ( $F_L$ )  
186 and rollover moment ( $M_R$ ) (Fig. 4). The side and lift forces acting on the truck were obtained by  
187 integrating the pressure distribution over the vertical and horizontal surfaces of truck. On the  
188 other hand, the rollover moment was calculated by summation of the moments of side and lift  
189 forces around point O (Fig. 4). The aerodynamic force and moment described above were  
190 transformed into non-dimensional coefficients by using the following equations:

$$\begin{aligned}
 C_s &= \frac{F_s}{\frac{1}{2} \rho U^2 A_s} \\
 C_L &= \frac{F_L}{\frac{1}{2} \rho U^2 A_s} \\
 C_R &= \frac{M_R}{\frac{1}{2} \rho U^2 A_s H}
 \end{aligned} \tag{5}$$

191 where  $\rho$  is the density of the air,  $1.18 \text{ kg/m}^3$ ;  $A_s$  is the side area of the truck,  $0.189 \text{ m}^2$ ;  $H$  is  
192 the reference height,  $0.262 \text{ m}$ ; and  $U$  is the mean streamwise wind speed measured at several  
193 heights above the ground according to the experimental study by Cheli et al. (2011a, b).  
194 Particularly,  $U$  was measured at the heights of  $0.25 \text{ m}$  and  $0.60 \text{ m}$  for the flat ground and  
195 embankment infrastructures, respectively.

196

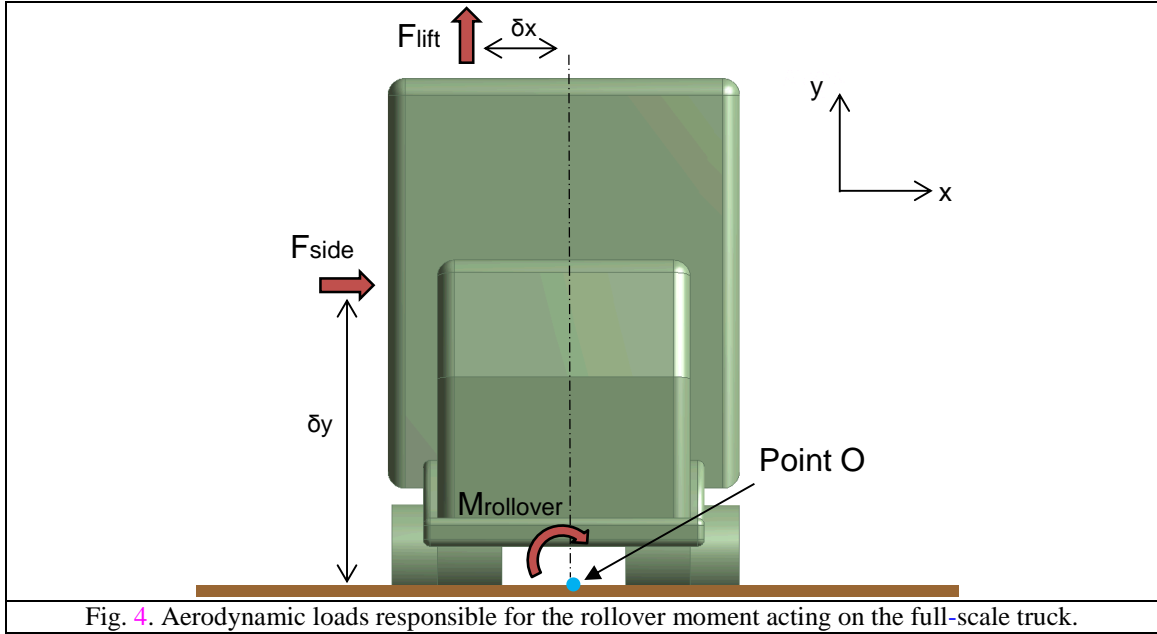


Fig. 4. Aerodynamic loads responsible for the rollover moment acting on the full-scale truck.

197

## 198 2.5. Design of experiments (DOE) methodology

199 The influence on the aerodynamic behavior of the truck of variables such as the slope angle  
 200  $\beta$  of the type-1 embankment and the horizontal distance  $d$  between the edge of the embankment  
 201 slope and the truck (See Fig. 1), were studied by means of a DOE. The type-1 embankment was  
 202 used for analysis instead of the type-2 because of its more unfavorable influence on the vehicle  
 203 stability, as can be seen in section 3.2. The first step in the DOE procedure (Del Coz Díaz et al.,  
 204 2012; Telenta et al., 2015) consists of selecting a method to determine the number of cases to  
 205 run and the values of the input variables for these cases. In this case, the Central Composite  
 206 Design (CCD) method was selected and then the different combinations of input values were  
 207 considered to obtain the predefined output variables.

208 The Response Surface models (RS-models) were developed based on the second order  
 209 polynomial regression models chosen as an approximation technique along with the results  
 210 obtained from the DOE method. As a part of the Response Surface Methodology (RSM), the  
 211 input variables  $x_1, x_2, \dots, x_n$  must be coded to compare their effects on truck stability. Factors  
 212 vary between -1 and +1, which corresponds to a variation between a minimum and a maximum  
 213 value in the coded scale, respectively. The second-order models obtained during the RSM  
 214 enable the identification of the critical points (maximum, minimum, or saddle) and can be  
 215 expressed in a general form as (Montgomery, 2001):

$$\hat{Y} = \alpha_0 + \sum_{i=1}^n \alpha_i x_i + \sum_{i=1}^n \alpha_{ii} x_i^2 + \sum_{i<j}^n \alpha_{ij} x_i x_j \quad (6)$$

216 where  $\hat{Y}$  is the predicted response variable;  $x_i$  denotes the coded values of the input  
 217 variables;  $\alpha_0, \alpha_i, \alpha_{ii}, \alpha_{ij}$  indicate the regression coefficients (offset term, main, quadratic  
 218 and interaction effects); and  $n$  is the number of variables studied. The regression coefficients are  
 219 determined by the Ordinary Least Squares (OLS) method. The OLS estimator is defined  
 220 according to the following expression (Montgomery, 2001; Del Coz Díaz et al., 2011):

$$\vec{\alpha}_{OLS} = \left( \begin{matrix} \vec{1}^T & \vec{X}^T \\ \vec{X} & \vec{X} \end{matrix} \right)^{-1} \begin{matrix} \vec{1}^T \\ \vec{X} \end{matrix} \vec{Y} \quad (7)$$

221 where  $\vec{\alpha}_{OLS}$  is a vector of regression coefficients;  $\vec{X}$  is an extended designed matrix for the  
 222 input variables including the coded levels; and  $\vec{Y}$  is a column vector of response variables that

223 includes the numerical simulation results for the combinations of input variable values  
 224 previously proposed by the DOE method. The input variables with their variation ranges  
 225 (maximum, minimum and current value) as well as the output variables, are shown in **Table 1**.  
 226 Finally, an optimization of the input variables was carried out by means of identifying the  
 227 combination of input variables values that minimized or maximized a given objective function.

228

229

Table 1. Ranges of input variables and response variables used in the DOE analyses.

Input variables	$\beta^a$ ( $^\circ$ )	$d^b$ (mm)	
Maximum	53	180	
Minimum	15	30	
Current	34	105	
Output variables	$Cf\_Side$	$Cf\_Lift$	$Cm\_Rollover$

<sup>a</sup>Angle of the type-1 embankment slope with the horizontal plane (see Fig. 1).

<sup>b</sup>Distance between the edge of the type-1 embankment slope and truck in full scale (see Fig. 1).

230

231

### 3. Results and discussion

232

233

#### 3.1. Reynolds number effect on aerodynamic response

234

235

236

237

238

239

240

241

242

243

244

In order to correctly obtain the aerodynamic loads acting on the full-scale truck, it is necessary that the dynamic similarity between the 1/10 scaled-down truck model and the full-scale truck is fulfilled. To satisfy the dynamic similarity criterion, the magnitudes of the Reynolds number  $Re$ , analyzed during the numerical simulation of the 1/10 scaled-down truck model should be equal to the full-scale truck case (Cermak and Isyumov, 1998; Kang and Lee, 2008). Therefore, to obtain the same value of  $Re$ , the wind speed should be 10 times the actual wind speed in the numerical simulation. None information about the fulfillment of the dynamic similarity criterion was indicated in Cheli et al. (2011a, b) so it was found interesting to check it in this section. Accordingly, the independence between the aerodynamic coefficients of the truck model and the  $Re$  values was assessed, since the actual wind velocity for the full scale truck was unknown.

245

246

247

248

249

250

For this study, flat ground was selected, because the part of the speed profile that influences the truck model does so at lower values of  $Re$  in this infrastructure. The aerodynamic coefficients of the truck model under cross wind conditions (yaw angle of  $90^\circ$ ) were obtained for five magnitudes of  $Re$  between  $2.5 \times 10^5$  and  $7.2 \times 10^5$ . The range of  $Re$  values proposed in this study includes the value used in the experimental tests. The  $Re$  values were obtained by using the following expression:

$$Re = \frac{\rho U_\infty L}{\mu} \quad (8)$$

251

252

253

254

255

256

257

where  $U_\infty$  is the undisturbed wind speed and  $L$  is the characteristic linear dimension whose value is equal to the reference height value defined for the aerodynamic coefficients. The aerodynamic coefficients of the truck model showed small variations in the range analyzed, as seen in Fig. 5. As the minimum value of Reynolds number defined in the numerical simulation for the studied scenarios was  $2.5 \times 10^5$ , it can be assumed that the dynamic similarity requirement is satisfied.



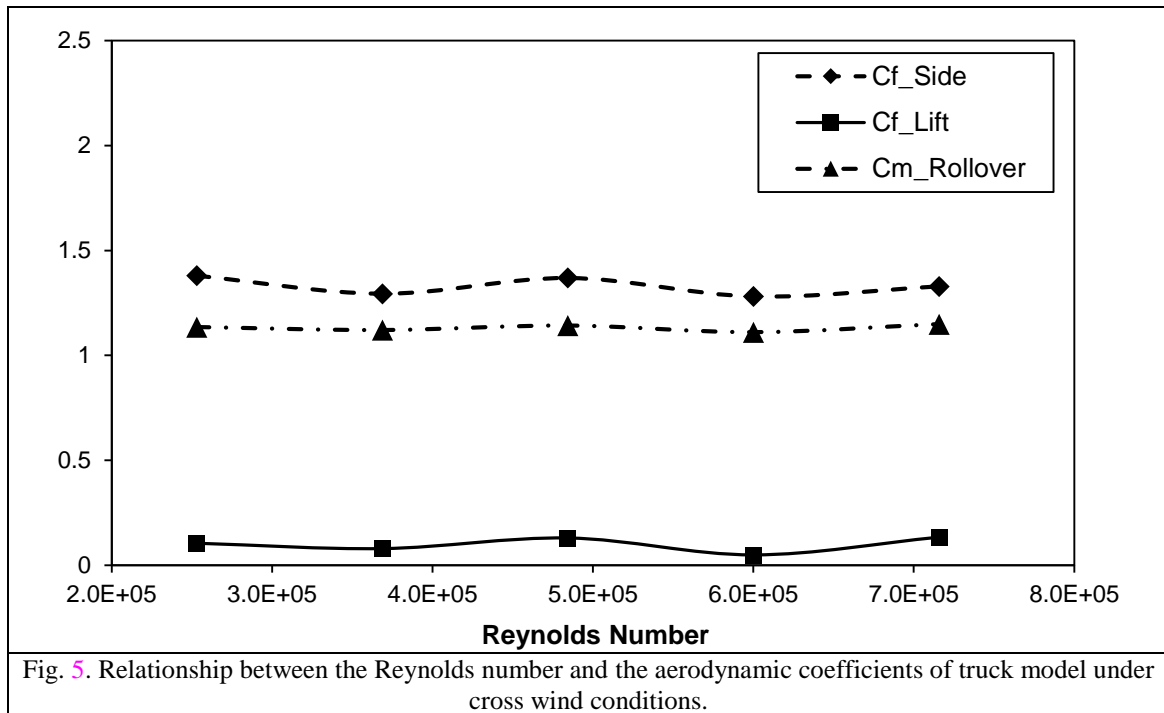
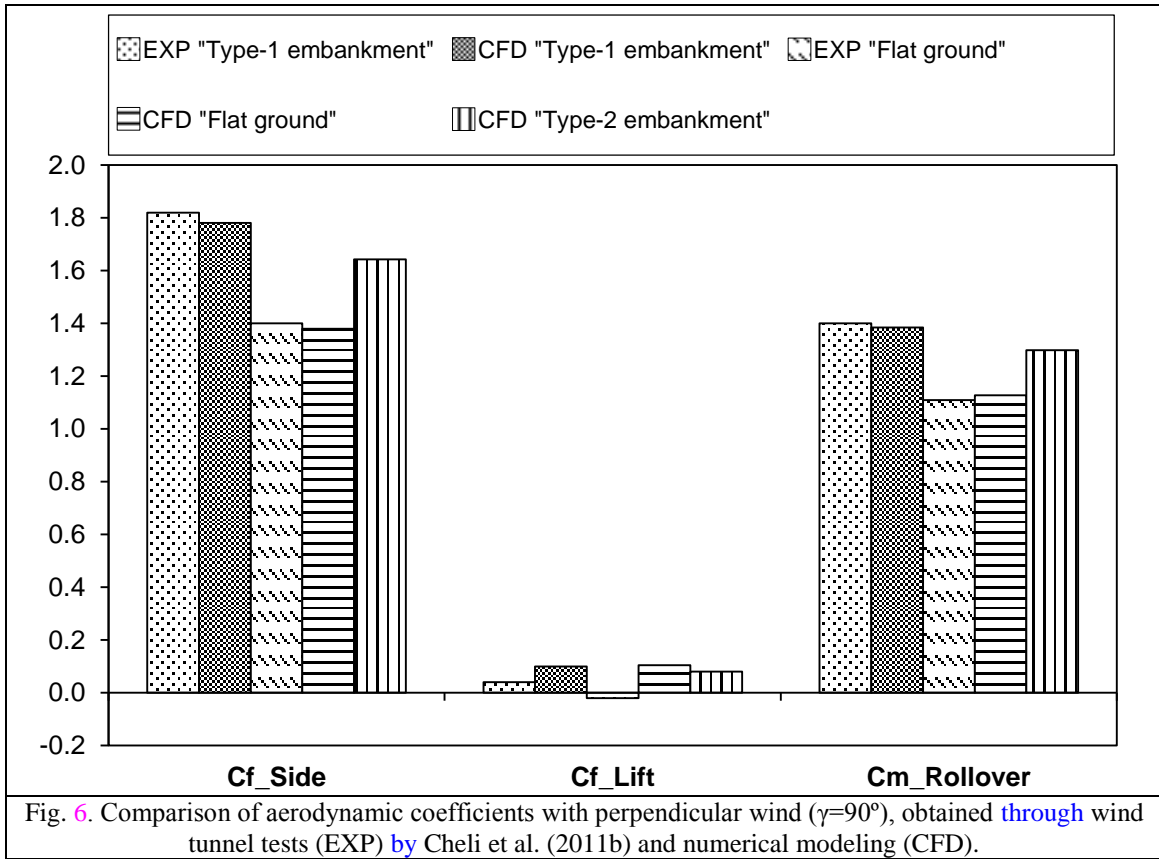


Fig. 5. Relationship between the Reynolds number and the aerodynamic coefficients of truck model under cross wind conditions.

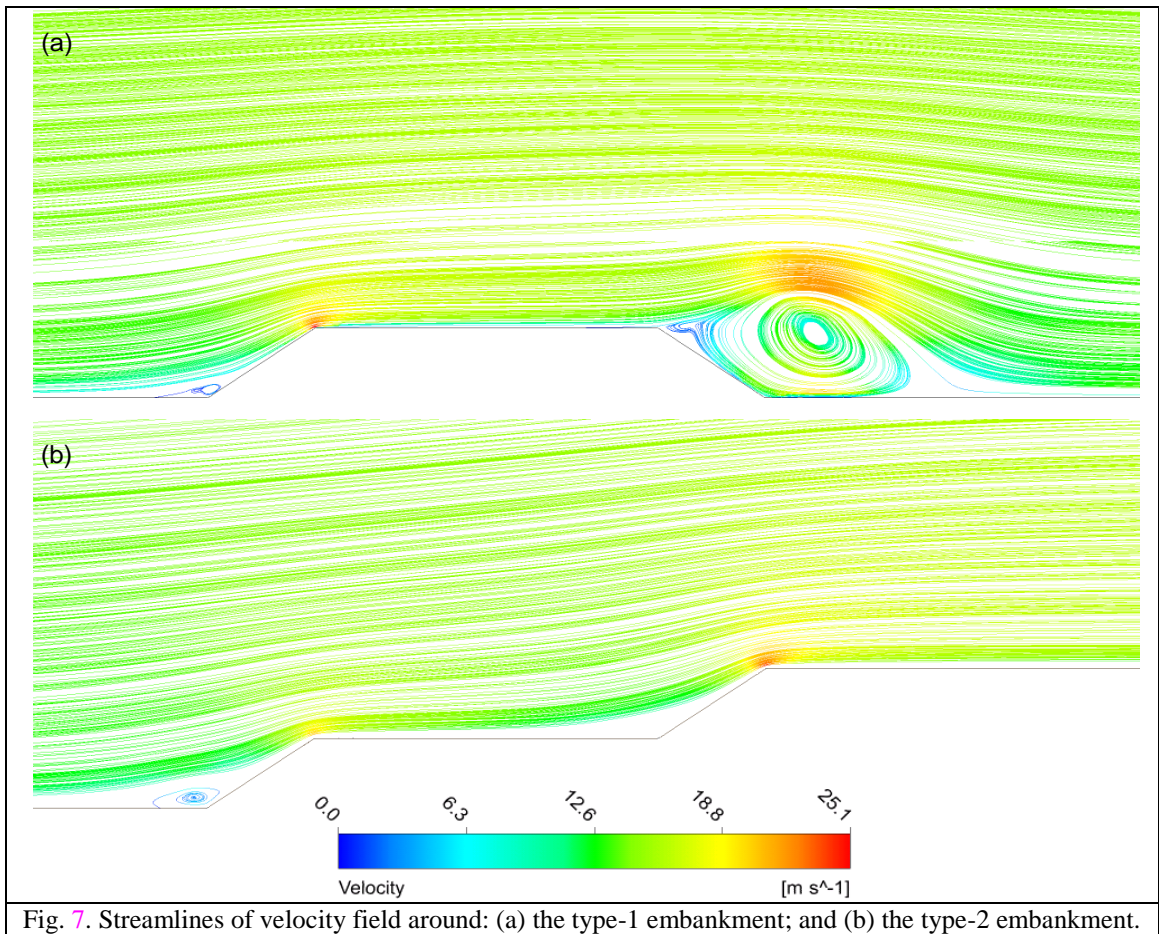
258

### 259 3.2. Influence of the embankment type

260 In order to analyze the influence of the embankment type on the stability of a truck model,  
 261 the aerodynamic coefficients of a truck were determined for flat ground, an embankment with  
 262 downward-slope on the leeward side (type-1 embankment) and an embankment with upward-  
 263 slope on the leeward side (type-2 embankment) (see Fig. 6). The rollover moment is the key  
 264 coefficient when the risk of suffering a rollover accident under cross wind conditions (Schober  
 265 et al., 2010) has to be evaluated; accordingly, the results indicate that the embankments affect  
 266 the truck stability more negatively than flat ground (see Fig. 6). This could be due to the slope  
 267 of the two embankments located on the upward side of the truck, because the slope causes a  
 268 decrease in the distance between the streamlines and consequently the air flow speed increases  
 269 (see Fig. 7). Specifically, the maximum velocity of the air flow is reached at the end of the  
 270 upward slope for both types of embankments. Therefore, the greatest differences in pressure  
 271 between the windward side and the leeward side of the truck are found for the embankments  
 272 (see Fig. 8). The most significant relative differences between the experimental reference values  
 273 and those from the numerical simulation were found for the lift aerodynamic coefficient (see  
 274 Fig. 6). However, in general, the aerodynamic coefficients obtained through both techniques  
 275 suggest the same conclusions regarding the infrastructures having a more detrimental influence  
 276 on the vehicle stability under cross wind conditions, as shown in Fig. 6.  
 277

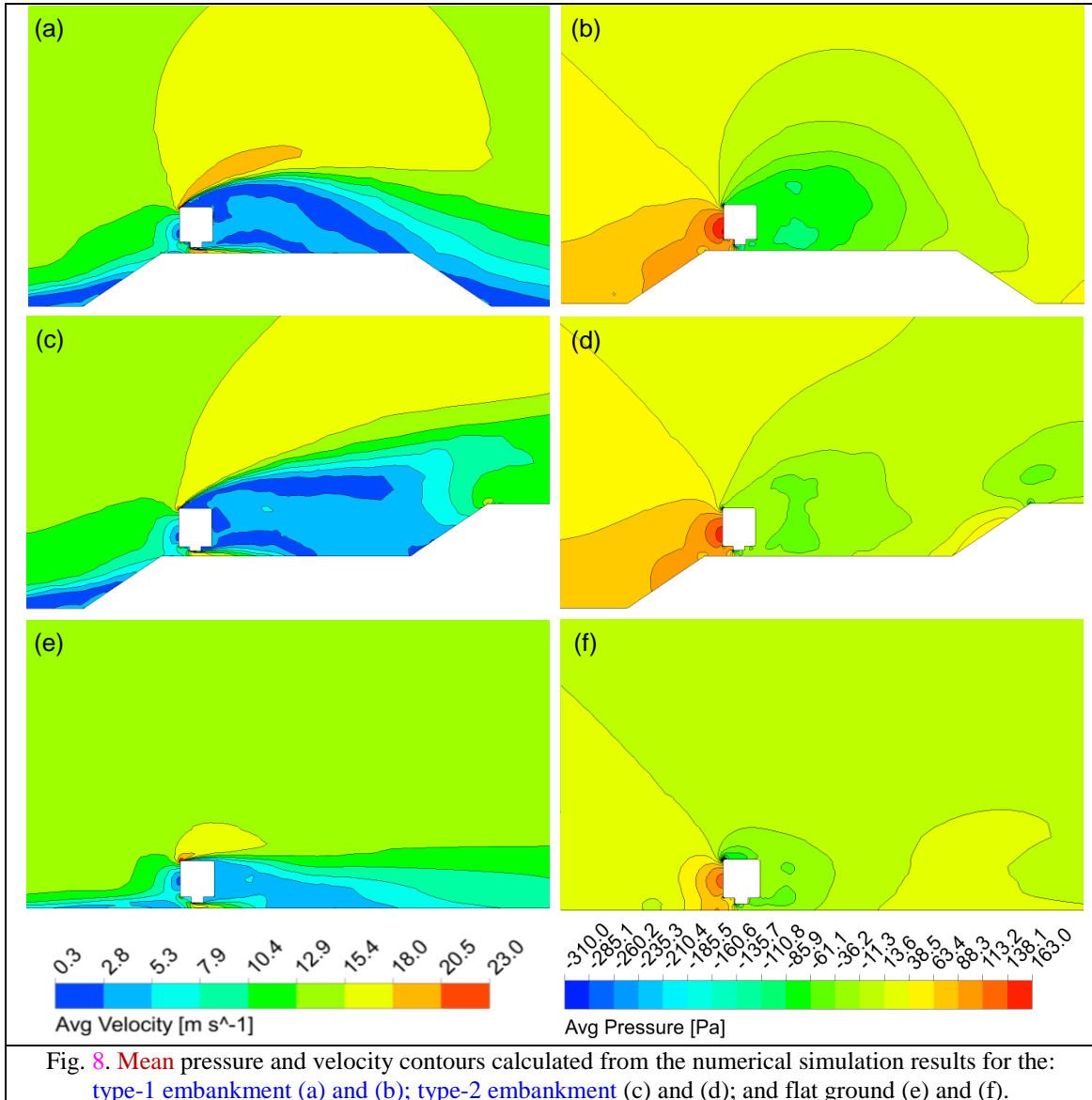


278



279

280 A higher value of the rollover coefficient was obtained for the type-1 embankment than for  
 281 the type-2 embankment. This is because the slope of the type-2 embankment on the leeward  
 282 side of the truck can slow down the wind speed in the air region between the truck and this  
 283 slope (Fig. 8). Therefore, the relative pressure values are closer to zero and as a consequence,  
 284 the suction force acting on the leeward surface of the truck is less on the type-2 embankment.  
 285 Regarding the lift coefficient, the small differences in pressure between the top and the bottom  
 286 of the truck for all the infrastructures are in agreement with the positive low values obtained for  
 287 the lift coefficient shown in Fig. 6.



288

### 289 3.3. Effect of the slope angle and the truck's position

290 During the DOE analysis, 9 numerical models were solved in order to determine the surface  
 291 response models. Figs. 9(a), 9(b) and 9(c) indicate the maximum variation undergone by the  
 292 aerodynamic coefficients of the truck studied as a function of the truck's position on the road,  
 293 and the slope angle, for the type-1 embankment (see Fig. 1). All the aerodynamic coefficients  
 294 are sensitive to variations both in the truck's position on the road and the slope angle (see Fig.  
 295 9). Particularly, a negative correlation exists between the aerodynamic coefficients and the  
 296 truck's position on road  $d$ . The increase in the aerodynamic coefficients with the decrease in the

297 distance between the truck and the embankment slope located on the windward side is due to  
298 the accelerated streamlines from the slope that hit a greater side surface of truck and flow closer  
299 to the top surface of truck.

300 On the other hand, the relationships between the aerodynamic coefficients and the slope  
301 angle are similar for the rollover moment and side force, but not for the lift force. In the case of  
302 the lift force, an increase in slope angle diminishes the coefficient whereas, in the case of the  
303 rollover moment and side force, the coefficients firstly increase with higher values of slope  
304 angle and then diminish (see Fig. 9). An increase in the slope angle moves the streamlines away  
305 from the top surface of the truck, and as a consequence, the lift force decreases. In addition, this  
306 increase of slope angle can accelerate the flow lines, narrowing the distance between them (see  
307 Fig. 7) and in turn allowing the increase in the side and rollover coefficients. However, these  
308 coefficients can also decrease at the highest values of the slope angle studied due to the  
309 streamlines from the slope hitting a smaller side surface of the truck. Therefore, both the side  
310 force and rollover moment versus slope angle may exhibit different trends depending on the  
311 range of the slope angle values studied, as shown in Fig. 9.

312 A lower risk a rollover accident is expected when an appropriate combination of input  
313 variables minimizes the rollover moment coefficient. Thus, the minimum rollover coefficient is  
314 1.23 and it is obtained for a truck position on the road of 180 mm (1800 mm in full scale) and a  
315 slope angle of 53°. Meanwhile, the worst combination of values from a rollover perspective was  
316 obtained for a truck position on the road of 30 mm (300 mm in full scale) and a slope angle of  
317 27.7°.

318  
319

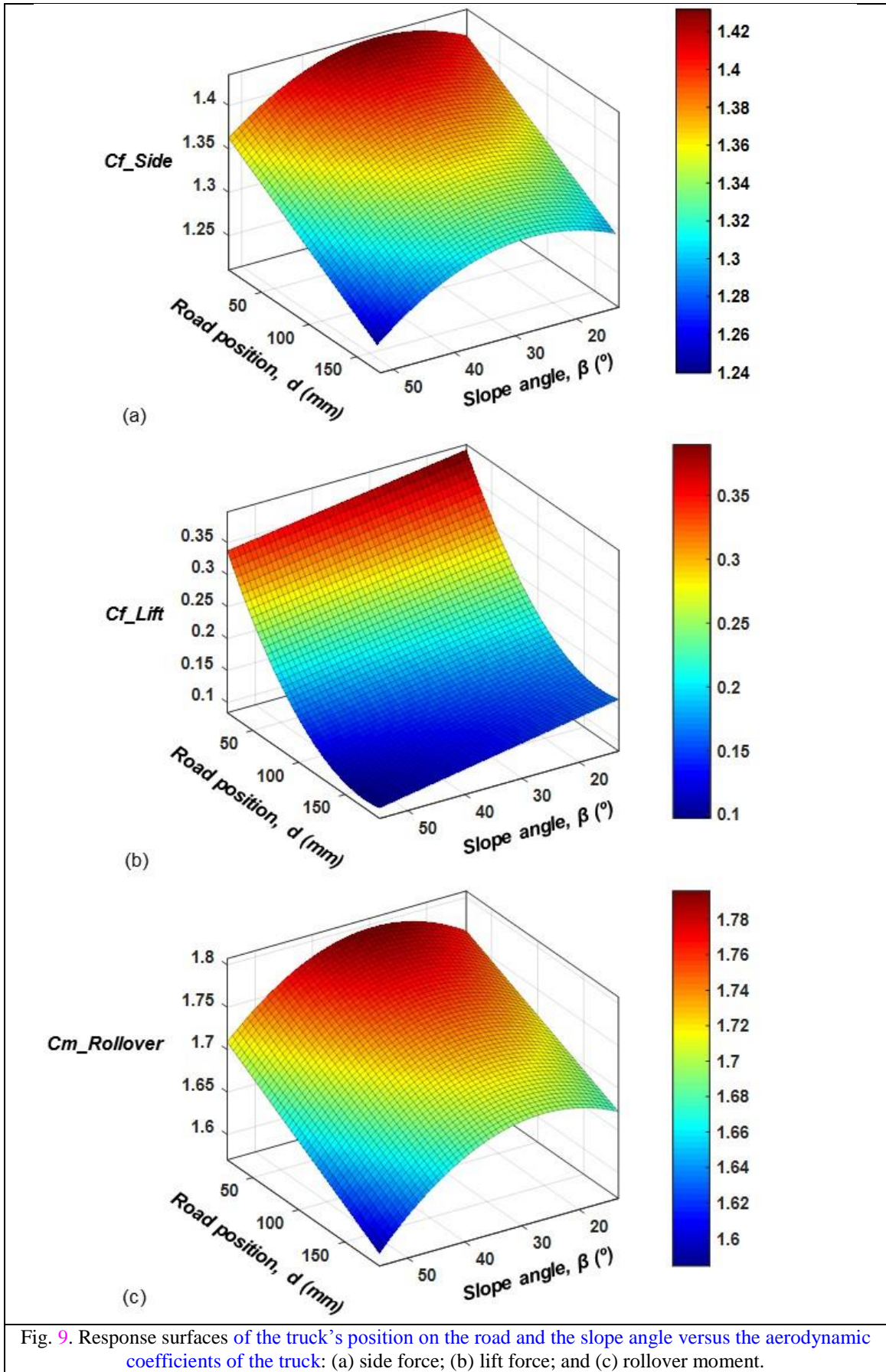


Fig. 9. Response surfaces of the truck's position on the road and the slope angle versus the aerodynamic coefficients of the truck: (a) side force; (b) lift force; and (c) rollover moment.

## 321 4. Conclusions

322 In this work, several numerical simulations were carried out to analyze the relationships  
323 between the aerodynamic coefficients of a truck and the type of road infrastructure. In addition,  
324 the effect of both the slope angle of an embankment and the truck position on the road on the  
325 aerodynamic response of the truck was studied. The main findings from the results are  
326 summarized as follows:

- 327 • Flat ground is the infrastructure where the rollover coefficient acting on the truck model  
328 shows the lowest values under cross wind conditions (yaw angle of 90°), while the  
329 highest values were obtained for the type-1 embankment.  
330
- 331 • A negative sensitivity of the rollover moment coefficient with respect to the truck's  
332 position on the road has been found. However, the sensitivity of the rollover moment  
333 coefficient to the slope angle can be negative or positive depending on the range of slope  
334 angle values considered.  
335
- 336 • The good agreement between the experimental and numerical results demonstrates that  
337 the LES approach in combination with the Finite Volume Method is a suitable  
338 methodology to estimate the vehicle's aerodynamic response.  
339
- 340 • The values of the truck's position on the road and the slope angle that optimize the  
341 vehicle stability were determined by applying the Response Surface Methodology.  
342
- 343 • The dynamic similarity between the 1/10 scaled-down truck model and a full-scale model  
344 can be considered to have been fulfilled according to the existing relationship between the  
345 aerodynamic coefficients and the Reynolds number.  
346
- 347 • The DOE procedure, when applied on a validated model, enables the saving of time and  
348 costs when manufacturing prototypes and carrying out field testing.  
349  
350

## 351 Acknowledgements

352 This work was supported by the OASIS Research Project, that was co-financed by the CDTI  
353 under the Ministry of Economy, Industry and Competitiveness) and developed by 16 Spanish  
354 companies: Iridium, OHL Concesiones, Abertis, Sice, Indra, Dragados, OHL, Geocisa, GMV,  
355 Asfaltos Augusta, Hidrofersa, Eipsa, PyG, CPS, AEC and Torre de Comares Arquitectos S.L;  
356 and 16 research centres. The authors would also like to thank the GICONSIME research group  
357 of the University of Oviedo (Spain) for their collaboration in this research. The authors also  
358 acknowledge the partial funding with FEDER funds under the Research Project FC-15-  
359 GRUPIN14-004.  
360



361 **References**

- 362 Alvarez-Legazpi, P., Vargas-Muñoz, M., Martínez-Acevedo, J. C., Botella-Malagón, J., and Rodríguez-  
363 Fernández, M. (2010). "Cross wind protection systems for high speed Railway Lines." *Proceedings of*  
364 *the ASME Joint Rail Conference 2010, JRC2010*, 133-143.
- 365 ANSYS Inc. *Fluent Manual Release 17.0*. (2017). Canonsburg, PA, USA.
- 366 Andersson, B., Andersson, R., Hakansson, L., Mortensen M., Rahman S., and Berend V. W. (2012).  
367 *Computational fluid dynamics for engineers*, Cambridge University Press, New York, USA.
- 368 Argentini, T., Ozkan, E., Rocchi, D., Rosa, L., and Zasso, A. (2011). "Cross-wind effects on a vehicle  
369 crossing the wake of a bridge pylon." *J.Wind Eng.Ind.Aerodyn.*, **99(6-7)**, 734-740.
- 370 Baker, C. J., and Reynolds, S. (1992). "Wind-induced accidents of road vehicles." *Accid Anal Prev.*,  
371 **24(6)**, 559-575.
- 372 Bettle, J., Holloway, A. G. L., and Venart, J. E. S. (2003). "A computational study of the aerodynamic  
373 forces acting on a tractor-trailer vehicle on a bridge in cross-wind." *J.Wind Eng.Ind.Aerodyn.*, **91(5)**,  
374 573-592.
- 375 Bitsuamlak, G. T., Stathopoulos, T., and Bédard, C. (2004). "Numerical evaluation of wind flow over  
376 complex terrain: Review." *J.Aerospace Eng.*, **17(4)**, 135-145.
- 377 Boccione, M., Cheli, F., Corradi, R., Muggiasca, S., and Tomasini, G. (2008). "Crosswind action on rail  
378 vehicles: Wind tunnel experimental analyses." *J.Wind Eng.Ind.Aerodyn.*, **96(5)**, 584-610.
- 379 Cermak, J. E., and Isyumov, N. (1998). *Wind Tunnel Studies of Buildings and Structures*. ASCE, Reston,  
380 Virginia.
- 381 Cheli, F., Corradi, R., Rocchi, D., Tomasini, G., and Maestrini, E. (2010). "Wind tunnel tests on train  
382 scale models to investigate the effect of infrastructure scenario." *J.Wind Eng.Ind.Aerodyn.*, **98(6-7)**,  
383 353-362.
- 384 Cheli, F., Corradi, R., Sabbioni, E., and Tomasini, G. (2011). "Wind tunnel tests on heavy road vehicles:  
385 Cross wind induced loads-Part 1." *J.Wind Eng.Ind.Aerodyn.*, **99(10)**, 1000-1010.
- 386 Cheli, F., Ripamonti, F., Sabbioni, E., and Tomasini, G. (2011). "Wind tunnel tests on heavy road  
387 vehicles: Cross wind induced loads-Part 2." *J.Wind Eng.Ind.Aerodyn.*, **99(10)**, 1011-1024.
- 388 Coleman, S. A., and Baker, C. J. (1990). "High sided road vehicles in cross winds." *J.Wind*  
389 *Eng.Ind.Aerodyn.*, **36(1-3)**, 1383-1391.
- 390 Del Coz Díaz, J. J., García Nieto, P. J., Castro-Fresno, D., and Menéndez Rodríguez, P. (2011). "Steady  
391 state numerical simulation of the particle collection efficiency of a new urban sustainable gravity  
392 settler using design of experiments by FVM." *Appl.Math.Comput.*, **217(21)**, 8166-8178.
- 393 Del Coz Díaz, J. J., Serrano López, M. A., López-Colina Pérez, C., and Álvarez Rabanal, F. P. (2012).  
394 "Effect of the vent hole geometry and welding on the static strength of galvanized RHS K-joints by  
395 FEM and DOE." *Eng.Struct.*, **41**, 218-233.
- 396 Delaunay, D., Baker, C. J., Cheli, F., Morvan, H., Berger, L., Casazza, M., Gomez, C., Cleac'h C.Le.,  
397 Saffell, R., Grégoire, R., and Vinuales, A. (2006). "Development of wind alarm systems for road and  
398 rail vehicles: presentation of the WEATHER project." *In: Proceedings of the SIRWEC2006, 13th*  
399 *International Riad Weather Conference*, Torino, Italy.

- 400 Diedrichs, B., Sima, M., Orellano, A., and Tengstrand, H. (2007). "Crosswind stability of a high-speed  
401 train on a high embankment." *Proc.Inst.Mech.Eng.Pt.F: J.Rail Rapid Transit*, **221(2)**, 205-225.
- 402 Dorigatti, F., Sterling, M., Rocchi, D., Belloli, M., Quinn, A. D., Baker, C. J., and Ozkan, E. (2012).  
403 "Wind tunnel measurements of crosswind loads on high sided vehicles over long span bridges."  
404 *J.Wind Eng.Ind.Aerodyn.*, **107-108**, 214-224.
- 405 Dragomirescu, E., Wang, Z., Hoftzyer, M.S. (2016). "Aerodynamic characteristics investigation of  
406 Megane multi-box bridge deck by CFD-LES simulations and experimental tests". *Wind and*  
407 *Structures, An International Journal*, **22(2)**, 161-184.
- 408 European Research Community on Flow, Turbulence and Combustion (ERCOFTAC). *Special Interest*  
409 *Group on Quality and Trust in Industrial CFD Best Practice Guidelines*, (2000). Eds. M. Casey and  
410 T. Wintergerste (online).
- 411 García, J., Muñoz-Paniagua, J., Jiménez, A., Migoya, E., Crespo, A., (2015). "Numerical study of the  
412 influence of synthetic turbulent in flow conditions on the aerodynamics of a train". *J. Fluid. Struct.*,  
413 **56**, 134–151.
- 414 He, X., Shi, K., Wu, T., (...), Wang, H., Qin, H (2016). "Aerodynamic performance of a novel wind  
415 barrier for train-bridge system". *Wind and Structures, An International Journal*, **23(3)**, 171-189.
- 416 Hibino, Y., Shimomura, T., and Tanifuji, K. (2010). "Full-Scale Experiment on the Behavior of a Railway  
417 Vehicle being subjected to Lateral Force". *J. Mech. Syst. Transp. Logist.*, **3**, 35-43.
- 418 Hoppmann, U., Koenig, S., Tielkes, T., and Matschke, G. (2002). "A short-term strong wind prediction  
419 model for railway application: Design and verification". *J.Wind Eng.Ind.Aerodyn.*, **90(10)**, 1127-1134.
- 420 Imai, T., Fujii, T., Tanemoto, K., Shimamura, T., Maeda, T., Ishida, H., and Hibino, Y. (2002). "New  
421 train regulation method based on wind direction and velocity of natural wind against strong winds".  
422 *J.Wind Eng.Ind.Aerodyn.*, **90(12-15)**, 1601-1610.
- 423 Kang, J. -H., and Lee, S. -J. (2008). "Experimental study of wind load on a container crane located in a  
424 uniform flow and atmospheric boundary layers". *Eng.Struct.*, **30(7)**, 1913-1921.
- 425 Kraichnan, R.H. (1970). "Diffusion by a random velocity field". *Phys Fluids*, **13(1)**, 22–31.
- 426 Ma, L., Zhou, D., Han, W., Wu, J., Liu, J. (2016). "Transient aerodynamic forces of a vehicle passing  
427 through a bridge tower's wake region in crosswind environment". *Wind and Structures, An*  
428 *International Journal*, **22(2)**, 211-234.
- 429 Madenci, E., and Guven, I. (2015). *The Finite Element Method and Applications in Engineering Using*  
430 *ANSYS*. Springer, New York.
- 431 Miao, X. J., Tian, H. Q., and Gao, G. J. (2010). "Effect of railway environment on aerodynamic  
432 performance of train on embankment". *Zhongnan Daxue Xuebao (Ziran Kexue Ban)/Journal of*  
433 *Central South University (Science and Technology)*, **41(5)**, 2028-2033.
- 434 Montgomery DC (2001). *Design and Analysis of Engineering Experiments*. John Wiley & Sons, New  
435 York.
- 436 Patankar SV, Spalding DB (1972). "A calculation procedure for heat, mass and momentum transfer in  
437 three-dimensional parabolic flows". *Int J Heat Mass Transf.*, **15(10)**: 1787-1806.
- 438 Schober, M., Weise, M., Orellano, A., Deeg, P., Wetzels, W., (2010). "Wind tunnel investigation of an  
439 ICE 3 endcar on three standard ground scenarios". *J.Wind Eng.Ind.Aerodyn.*, **98(6-7)**, 345-352.

- 440 Shao, X.M., Wan, J., Chen, D.W., Xiong, H.B., (2011). “Aerodynamic modeling and stability analysis of  
441 a high-speed train under strong rain and crosswind conditions”. *Journal of Zhejiang University:  
442 Science A*. **12(12)**, 964-970.
- 443 Smagorinsky J., (1963). “General circulation experiments with the primitive equations. I”. The basic  
444 experiment. *Mon Weather Rev*, **91**, 99–164.
- 445 Smirnov, R., Shi, S., Celik, I. (2001). “Random flow generation technique for large eddy simulations and  
446 particle-dynamics modelling”. *J Fluids Eng*, **123**, 359–371.
- 447 Sterling, M., Quinn, A.D., Hargreaves, S.D., Cheli, F., Sabbioni, E., Tomasini, G., Delaunay, D.,  
448 Baker, C. J., Morvan, H., (2010). “A comparison of different methods to evaluate the wind induced  
449 forces on a high sided lorry”. *J.Wind Eng.Ind.Aerodyn.* **98(1)**, 10-20.
- 450 Suzuki, M., Tanemoto, K., Maeda, T. (2003). Aerodynamic characteristics of train/vehicles under cross  
451 winds. *J.Wind Eng.Ind.Aerodyn.*, **91(1-2)**, 209-218.
- 452 Telenta, M., Batista, M., Biancolini, M.E., Prebil, I., Duhovnik, J. (2015). “Parametric numerical study of  
453 wind barrier shelter”. *Wind and Structures, An International Journal*, **20(1)**, 75-93.
- 454 Tsubokura, M., Nakashima, T., Kitayama, M., Ikawa, Y., Hee-Doh, D., and Kobayashi, T. (2010). “Large  
455 eddy simulation on the unsteady aerodynamic response of a road vehicle in transient crosswinds”. *Int.  
456 J.Heat Fluid Flow*, **31 (6)**, 1075–1086.
- 457 Tu J, Yeoh GH, Liu C (2012). *Computational Fluid Dynamics. A Practical Approach*, 2nd Edition.  
458 Butterworth-Heinemann, Oxford.
- 459 Wang, B., Xu, Y.L., Zhu, L.D. and Li Y.L. (2014). “Crosswind effect studies in road vehicle passing by  
460 bridge tower using computational fluid dynamics”. *Eng. Appl. Comput. Fluid Mech.*, **8(3)**, 330-344.  
461
- 462 Wu, M., Li, Y., Zhang, W. (2017). “Impacts of wind shielding effects of bridge tower on railway vehicle  
463 running performance”. *Wind and Structures, An International Journal*, **25(1)**, 63-77.  
464
- 465 Yang, Y., Xie, Z., Gu, M. (2017). “Consistent inflow boundary conditions for modelling the neutral  
466 equilibrium atmospheric boundary layer for the SST k- $\omega$  model”. *Wind and Structures, An  
467 International Journal*, **24(5)**, 465-480.  
468
- 469 Yang, S., Xiang, H., Fang, C., Wang, L., Li, Y. (2017). “Wind tunnel tests on flow fields of full-scale  
470 railway wind barriers”. *Wind and Structures, An International Journal*, **24(2)**, 171-184.